J. Fluid Mech. (1972), *vol.* 54, *part* 1, *pp.* 163–187
Printed in Great Britain

Nonlinear motions induced by moving thermal waves

By RICHARD E. YOUNG, GERALD SCHUBERT
Department of Planetary and Space Science, University of California, Los Angeles
AND KENNETH E. TORRANCE
Department of Thermal Engineering, Cornell University

(Received 22 December 1971)

The motion induced in a layer of Boussinesq fluid by moving periodic thermal waves is obtained by numerically solving the complete nonlinear two-dimensional momentum and temperature equations. Three sets of boundary conditions are treated: rigid upper and lower boundaries with symmetrical heating; free upper boundary and rigid lower boundary with heating only at the top; free upper and lower boundaries with symmetrical heating. The nonlinear streamline patterns show that, when the velocity fluctuations are larger than the phase speed of the thermal wave and the mean flow, the convection cells have shapes governed by fluctuating nonlinear interactions. Significant mean velocities can be created even without the characteristic tilt in the convection cells expected on the basis of linear theory. Nonlinear interactions can lead to a mean shear even in the absence of motion of the thermal source. When the viscous diffusion time across the fluid layer is less than or of the same order as the period of the thermal wave, the order of magnitude of the induced mean velocity does not exceed that of the phase speed of the wave, even for intense thermal forcing.

1. Introduction

The situation in which a travelling thermal wave can generate a mean shear within a layer of fluid has interest both as a purely fluid-dynamical problem and as a possible explanation for the observed four-day retrograde zonal motion of the upper atmosphere of Venus. A significant body of literature discussing mean flows induced by thermal waves exists, but the treatments have been mainly limited to the linear regime, or to situations wherein the mean-field approximation to the Navier–Stokes equations could be applied.

Linear treatments of the problem have been carried out by Stern (1959), Davey (1967), Malkus (1970), Kelly & Vreeman (1970), Schubert, Young & Hinch (1970), Hinch & Schubert (1971) and Whitehead (1971). The results of these linear investigations have shown that the mean flow induced in a layer of fluid by a travelling thermal wave is proportional to the square of the amplitude of the wave. The mean shear is supplied by correlations of the fluctuating components of the horizontal and vertical velocities, these correlations giving rise to a transport of horizontal momentum in the direction of the mean shear.

Some nonlinear aspects of the problem have been treated using the mean-field

approximation to the Navier–Stokes equations (Schubert 1969; Hinch & Schubert 1971). The mean-field approximation involves assuming that the mean flow is large compared with the velocity fluctuations, neglecting the nonlinear interactions involving the fluctuating quantities, but retaining the nonlinear interactions of mean quantities with fluctuating ones. The analysis by Schubert (1969) considered situations where the thermal forcing was large, but unfortunately the amplitude of the horizontal velocity fluctuation in these instances was of the same order as the mean flow, probably rendering the mean-field approximation invalid. In the investigation by Hinch & Schubert (1971) there were restrictions limiting the thermal wave amplitude, however, it was found that the mean flow could still be larger than the phase speed of the thermal wave when the fluid viscosity was sufficiently small.

It is the purpose of the present study to investigate the possibility of producing large mean flows when the thermal forcing becomes large but the fluid viscosity is not necessarily small. Further, we wish to observe the effects of different boundary conditions on the flow field, because not only can the qualitative behaviour of the mean velocity be affected by boundary conditions, but the entire flow pattern can exhibit interesting differences. The model we consider is a two-dimensional, horizontally infinite layer of fluid bounded above and below by plane surfaces. The full nonlinear Boussinesq two-dimensional momentum and temperature equations are solved numerically for the following three sets of boundary conditions: (i) rigid top and bottom boundaries with heating applied symmetrically at the boundaries; (ii) free top and bottom boundaries with heating applied symmetrically at the boundaries; (iii) free upper boundary, rigid lower boundary and heating only at the top. The reason for choosing the first set of boundary conditions was that the results of Hinch & Schubert (1971) showed that under the conditions for which their analysis is valid the mean velocity is still proportional to the square of the thermal wave amplitude well beyond the linear regime. It appeared, therefore, that it might be possible to extend the linear expressions for the mean velocity to very nonlinear situations. The second set of boundary conditions was chosen for comparison with the rigid–rigid case. The third set of boundary conditions is of interest because of the results of Schubert *et al.* (1970), namely that for these conditions the mean velocity changes sign depending on the ratio of the diffusion rate of temperature to the diffusion rate of momentum.

A formal statement of the problem is presented in § 2, followed by a description of the numerical procedure in § 3. Section 4 gives the range of parameter values considered and § 5 discusses general aspects of the flow field. Sections 6–10 present the nonlinear results.

2. Detailed model

The basic model investigated is shown in figure 1. An initially isothermal layer of Boussinesq fluid of thickness d extending to $\pm\infty$ in the x direction is subjected to a periodic travelling thermal wave of the form $A\cos(kx+\omega t)$, A being measured from the constant initial temperature of the fluid, and k and ω being, respectively, the wavenumber and angular frequency of the wave. Let the velocity be

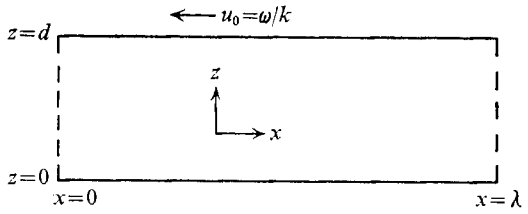

FIGURE 1. Model geometry. λ is the wavelength of the thermal wave.

$\mathbf{u} = (u, 0, w)$. The equations of motion are formulated in terms of a stream function ψ and the vorticity Ω.

$$u = -\partial\psi/\partial z, \quad w = \partial\psi/\partial x, \tag{2.1}$$

$$\Omega = \partial u/\partial z - \partial w/\partial x. \tag{2.2}$$

The equations of motion, together with the temperature equation, are

$$\nabla^2\psi = -\Omega, \tag{2.3}$$

$$\frac{\partial\Omega}{\partial t} + \frac{\partial(u\Omega)}{\partial x} + \frac{\partial(w\Omega)}{\partial z} = -g\alpha\frac{\partial T}{\partial x} + \nu\nabla^2\Omega, \tag{2.4}$$

$$\frac{\partial T}{\partial t} + \frac{\partial(uT)}{\partial x} + \frac{\partial(wT)}{\partial z} = \kappa\nabla^2 T, \tag{2.5}$$

where T is the temperature, g the gravitational acceleration, α the thermal coefficient of expansion, ν the kinematic viscosity and κ the thermal diffusivity.

If the vorticity equation is averaged over a wavelength in the x direction (averaged quantities being denoted by a bar), we get

$$\frac{\partial\bar{\Omega}}{\partial t} + \frac{\partial(\overline{w\Omega})}{\partial z} = \nu\frac{\partial^2\bar{\Omega}}{\partial z^2}, \tag{2.6}$$

where $\bar{\Omega} = \partial\bar{u}/\partial z$ is the mean shear. The mean flow is thus produced by correlations of the fluctuating components of the velocity, i.e. by Reynolds stresses set up within the fluid. In the steady state this momentum transport of the Reynolds stresses must be balanced by the viscous diffusion of mean momentum. A similar equation can be derived for the mean temperature $\bar{T}$:

$$\frac{\partial\bar{T}}{\partial t} + \frac{\partial}{\partial z}(\overline{wT}) = \kappa\frac{\partial^2\bar{T}}{\partial z^2}. \tag{2.7}$$

The three sets of boundary conditions considered are the following.

(i) Rigid–rigid:

$$\left.\begin{aligned} &u = w = 0 \quad \text{at} \quad z = 0, d, \\ &T = A\cos(kx + \omega t) \quad \text{at} \quad z = 0, d. \end{aligned}\right\} \tag{2.8}$$

(ii) Free–free:

$$\left.\begin{aligned} &w = du/dz = 0 \quad \text{at} \quad z = 0, d, \\ &T = A\cos(kx + \omega t) \quad \text{at} \quad z = 0, d. \end{aligned}\right\} \tag{2.9}$$

(iii) Free–rigid

$$\left.\begin{aligned} w &= \begin{cases} du/dz = 0 & \text{at} \quad z = d, \\ u = 0 & \text{at} \quad z = 0, \end{cases} \\ T &= \begin{cases} A\cos(kx+\omega t) & \text{at} \quad z = d, \\ 0 & \text{at} \quad z = 0. \end{cases} \end{aligned}\right\} \tag{2.10}$$

The problem is non-dimensionalized using ω^{-1} as the time scale, k^{-1} as the horizontal length scale, d as the vertical length scale and A as the temperature scale; this yields the four dimensionless parameters

$$F = (gd/u_0^2)\,\alpha A, \quad S = \omega d^2/\nu, \quad P = \nu/\kappa, \quad \beta = kd,$$

where $u_0 = \omega/k$. The parameter F represents the ratio of buoyancy forces to inertial forces, S is 2π times the ratio of the viscous diffusion time across the fluid layer to the period of the wave, P is the Prandtl number and β is 2π times the ratio of the fluid-layer thickness to the wavelength of the wave.

The governing non-dimensional equations are (Ω being scaled with u_0/d, ψ scaled with $u_0 d$)

$$\nabla_\beta^2 \psi = -\Omega, \tag{2.11}$$

$$u = -\partial\psi/\partial z, \quad w = \partial\psi/\partial x, \tag{2.12}$$

$$\frac{\partial\Omega}{\partial t} + \frac{\partial(u\Omega)}{\partial x} + \frac{\partial(w\Omega)}{\partial z} = -F\frac{\partial T}{\partial x} + \frac{1}{S}\nabla_\beta^2\Omega, \tag{2.13}$$

$$\frac{\partial T}{\partial t} + \frac{\partial(uT)}{\partial x} + \frac{\partial(wT)}{\partial z} = \frac{1}{SP}\nabla_\beta^2 T, \tag{2.14}$$

where $\nabla_\beta^2 = \beta^2(\partial^2/\partial x^2) + (\partial^2/\partial z^2)$. In order to facilitate determination of when the steady state was reached, the equations were solved in the frame of reference moving with the applied thermal wave. Henceforth all variables are understood to be dimensionless.

3. Numerical procedure

Most of the numerical techniques used are described in some detail by Torrance (1968) and Torrance & Rockett (1969). The reader is therefore referred to these papers for discussion of many statements in this section not specifically referenced.

The grid system used is shown in figure 2. All quantities were evaluated at each grid point. All linear spatial derivatives were approximated by standard three-point central differences, while the time derivatives were approximated by one-sided forward differences. With $x = (i-1)\Delta x$, $z = (j-1)\Delta z$, the vertical convective derivative was approximated by a centred difference

$$\left(\frac{\partial(wf)}{\partial z}\right)_{i,j} = [(wf)_{i,j+1} - (wf)_{i,j-1}]/2\Delta z + O(\Delta z^2). \tag{3.1}$$

This form of differencing is stable if $\Delta z \lesssim 8/Sw$ at any grid point (assuming $P \leqslant 1$); for the range of parameter values considered in this study the stability

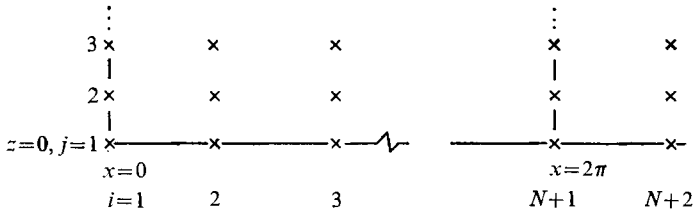

FIGURE 2. Numerical grid system.

condition was satisfied. The criterion for the same form of differencing in the horizontal is $\Delta x \lesssim 8\beta^2/Su$. Since u is $O(1)$ or larger and β is small it was not feasible to satisfy this criterion for the values of S which we wanted to consider. Hence we approximated the horizontal convective derivative by

$$\left(\frac{\partial(uf)}{\partial x}\right)_{i,j} = \frac{1}{\Delta x}\left[\frac{u_{i+1,j}+u_{i,j}}{2} f_{i,j} - \frac{u_{i,j}+u_{i-1,j}}{2} f_{i-1,j}\right] \tag{3.2}$$

when $(u_{i+i,j}+u_{i,j})$ and $(u_{i,j}+u_{i-1,j})$ were positive and by

$$\left(\frac{\partial(uf)}{\partial x}\right)_{i,j} = \frac{1}{\Delta x}\left[\frac{u_{i+1,j}+u_{i,j}}{2} f_{i+1,j} - \frac{u_{i,j}+u_{i-1,j}}{2} f_{i,j}\right] \tag{3.3}$$

when the same quantities were negative. When one was positive and the other negative an appropriate combination was used.

The above form of the horizontal convective derivative worked quite well for the cases where there was symmetry in the vertical, for example, when the upper and lower surfaces were rigid no-slip boundaries and the thermal fluctuations were applied symmetrically to each surface. However, in the free–rigid case there were accuracy problems in computing the mean velocity using this convective approximation. If one does an analysis of this form of the differencing it is found that there exist artificial numerical Reynolds stresses of $O(\Delta x)$. These artificial Reynolds stresses result when the finite-difference form of the vorticity equation is averaged over a wavelength in the x direction. Evidently, in the symmetric cases these errors tend to cancel, but in asymmetric situations they do not. Hence, for the free–rigid case it was preferable to use a central difference for the horizontal advective term and ensure numerical stability by adding an artificial horizontal viscous term of $O(\Delta x)$. In fact, this amounts to adding a term $\nu_N(z)\,\partial^2\Omega/\partial x^2$ to the differential equation governing Ω, where ν_N is the artificial viscosity, being proportional to the maximum horizontal velocity at a given z and the grid spacing Δx. In the first difference form mentioned for the horizontal advective term there is also an $O(\Delta x)$ artificial viscous term. The advantage of the second form is that the numerical viscosity can be made independent of x, so that no artificial Reynolds stress results from this term, i.e.

$$\overline{\nu_N \frac{\partial^2\Omega}{\partial x^2}} = 0.$$

The reason for using either of the above forms for the horizontal convective differencing is that there is no grid size restriction on Δx necessary to ensure numerical stability.

Since all quantities are periodic in x it was only necessary to extend one extra vertical column of grid points outside the x interval of $(0, 2\pi)$ to handle the boundaries at $x = 0$ and $x = 2\pi$. The treatment of the boundaries at $z = 0, 1$ was as follows. Since the stream function is constant in x along $z = 0, 1$, ψ can be set equal to zero at $z = 0$. However, since there is a mean flow in the problem, ψ cannot be prescribed at $z = 1$. From the horizontal momentum equation it is easy to show that

$$\frac{\partial \psi(z=1)}{\partial t} = \frac{1}{S}[\bar{\Omega}(z=0) - \bar{\Omega}(z=1)]. \tag{3.4}$$

Since $\Omega = 0$ at a free surface, it is only necessary to consider further the boundary values of Ω at rigid surfaces. This was accomplished by expanding ψ in a Taylor series about the rigid boundary, using the velocity boundary conditions, and noting that at a rigid surface

$$\partial^2\psi/\partial z^2 = -\Omega, \tag{3.5}$$

and

$$\partial^3\psi/\partial z^3 = -\partial\Omega/\partial z. \tag{3.6}$$

By approximating $\partial\Omega/\partial z$ by a one-sided difference using the grid point immediately adjacent to the rigid boundary, the boundary value of Ω was obtained to $O(\Delta z^2)$ in terms of ψ and Ω at the adjacent grid point. There are no problems regarding the boundary values of the temperature of course, since these are already prescribed.

The numerical procedure was as follows. Starting from given initial conditions the temperature was advanced in time.

$$T_{t+\Delta t} = T_t + \Delta t \text{ [finite-difference approximation of spatial derivatives]}.$$

Then, using the known values of temperature at $t + \Delta t$, the vorticity equation was advanced in time. By averaging the vorticity at the boundaries $z = 0, 1$ the stream function at $z = 1$ was determined. With the boundary values of ψ and the interior values of Ω known, the elliptic equation for ψ was solved by the method of successive over-relaxation. When the current values of the stream function and the vorticity at all interior grid points were known the new values of Ω at the rigid boundaries could be computed as described above. The new velocities required for the convective derivatives were obtained from centred differences of the stream function; this completed the cycle.

The time step at each point was limited by numerical stability considerations. At each grid point

$$\Delta t \leqslant \left[\frac{(u_{i,j} + u_{i+1,j})}{2} + \frac{2}{SP\Delta z^2} + \frac{2\beta^2}{SP\Delta x^2}\right]^{-1} \tag{3.7}$$

when the first form of the horizontal convective derivative was used and $(u_{i,j} + u_{i+1,j}) > 0$, or

$$\Delta t \leqslant \left[\max_i \frac{|u|}{2} + \frac{2}{SP\Delta z^2} + \frac{2\beta^2}{SP\Delta x^2}\right]^{-1}, \tag{3.8}$$

when the second form of the horizontal convective derivative was used. If the Prandtl number is greater than unity, then the factor P does not appear in the time restriction. The above inequalities applied to all interior grid points. However, a numerical instability was encountered in obtaining the vorticity at

the rigid surfaces, and the elimination of this required reducing the time step somewhat from that given in the above criteria.

The successive over-relaxation method used to solve for the stream function is the most time consuming part of the calculation; however, except for the very early stages of flow development, ψ relaxed to within a specified tolerance limit in less than 10 iterations, even for fine grid spacing. Thus successive over-relaxation was probably more efficient in this case than solving for ψ using fast Fourier transforms. The maximum number of interior grid points used in obtaining steady-state values was 800 (20 vertical, 40 horizontal). This represented what we felt was an acceptable compromise between accuracy and computer time. Spot checks of accuracy, however, were made using more refined grids.

As a final note on the differencing procedure, it should be pointed out that the finite-difference forms of the continuity, vorticity and energy equations are conservative, i.e. if the equations are summed over all interior grid points, there are, respectively, no false numerical sources or sinks of mass, vorticity, or energy.

4. Parameter values

Most of the literature has treated situations where $\beta \ll 1$. For comparison purposes we also consider a small value of β, namely $\beta = 10^{-2}$, in all the computations. In the rigid–rigid cases results are presented for $P = 0{\cdot}1$ and $1{\cdot}0$. The value $P = 1{\cdot}0$ is representative of many gases and $P = 0{\cdot}1$ was chosen to investigate the increase in $\bar{u}$ as P becomes small. For each value of P, F ranges from 1 to 100 and S varies from 10 to 50. In certain instances F is extended up to 400. The mean velocity in all cases increases as F and S increase. However, to extend the range of these parameters accurately to significantly larger values would require considerable computer time, or in some instances would not be feasible owing to the onset of turbulence. Below $F = 1{\cdot}0$ or $S = 10$ new physical effects are not anticipated, so these seemed reasonable lower limits.

Except for the Prandtl number, the same parameter values are used for free–rigid boundary conditions. In the linear approximation the critical Prandtl number P_c for the vertically averaged mean flow $\tilde{u}$ ($\tilde{u}$ reverses sign at $P = P_c$, see § 5) is between $0{\cdot}1$ and $0{\cdot}3$ when $10 \gtrsim S \gtrsim 50$. Since it is of interest to observe nonlinear effects on P_c, results for free–rigid boundary conditions are presented for $P = 0{\cdot}1$ and $0{\cdot}3$. As a comparison with rigid–rigid boundaries using symmetric heating, free–free symmetric heating results are presented only at $S = 10$, $P = 1{\cdot}0$, with F varying from 1 to 200.

In the following sections of the paper, if the value of S is not specifically given the value $S = 10$ is implied.

5. General aspects of the flow

In this section we briefly summarize particular characteristics of linear theory and certain general features of the flow. As mentioned in the introduction, linear analysis predicts the velocity fluctuations to be proportional to F and the mean

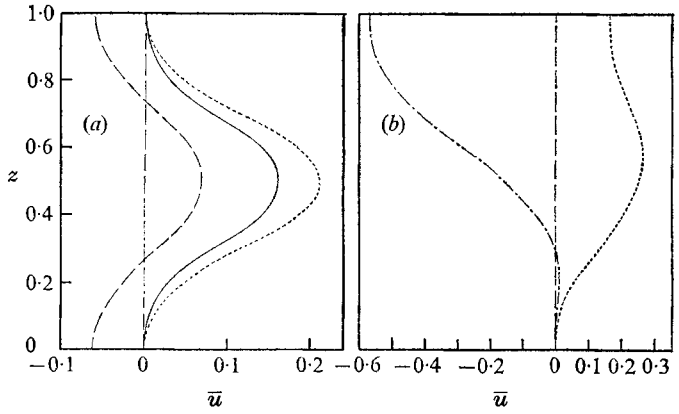

FIGURE 3. Steady-state mean velocity profiles at $F = 100$. (*a*) – – – –, free–free, $P = 1{\cdot}0$; ——, rigid–rigid, $P = 1{\cdot}0$; - - - - -, rigid–rigid, $P = 0{\cdot}1$. (*b*) — — — — —, free–rigid, $P = 0{\cdot}3$; - - - - -, free–rigid, $P = 0{\cdot}1$.

flow to be proportional to F^2, irrespective of the specific thermal or velocity boundary conditions. The velocity fluctuations and the mean velocity are independent of β to $O(\beta^2)$ (when β is small). In the rigid–rigid case $\bar{u}$ is everywhere greater than or equal to zero for all values of S and P, while for free–free boundary conditions $\bar{u}$ is positive at the channel centre but negative at the horizontal boundaries, such that there is no net momentum within the fluid layer. For free–free boundaries the fluid can acquire no net momentum if there is none initially.

According to linear theory the mean flow at a given z in the free–rigid case is positive or negative depending on the specific values of S and P. This behaviour leads to the existence of a critical Prandtl number P_c for the vertically averaged mean velocity $\tilde{u}$. For $P < P_c$, $\tilde{u} > 0$ and for $P > P_c$, $\tilde{u} < 0$. When S is small P_c is independent of S, but when S is large P_c varies as $S^{-\frac{3}{2}}$. It should be noted that when $\tilde{u}$ is positive (negative), part of the mean velocity profile can still be negative (positive).

The general dependence of the mean velocity on S and P in the linear regime is quite complicated, but in certain limits the expressions reduce to relatively simple algebraic formulae. Since the parameters to be considered in this study do not correspond to any of these limits, the algebraic formulae will not be presented here, but the interested reader is referred to the papers mentioned in § 1.

Figure 3 (*a*) shows typical steady-state mean velocity profiles for rigid–rigid and free–free boundary conditions for $F = 100$ and different values of P. These profiles are symmetric about the channel centre (remember that symmetric heating is applied in these cases). Mean velocity profiles for the free–rigid case at $F = 100$ and $P = 0{\cdot}1$, $0{\cdot}3$ are shown in figure 3 (*b*). The structure of the free–rigid profile can probably be explained as being due to the increased influence of thermal tilting as the top of the channel is approached (Schubert *et al.* 1970). As the Prandtl number decreases, this effect will be considerably less, and as the Prandtl number becomes large the entire profile tends to negative values. Because of this 'jet' structure in the free–rigid case, when P is somewhere between $0{\cdot}1$ and $0{\cdot}3$, $\bar{u}(1)$ can be negative although at the same time $\tilde{u}$ is positive.

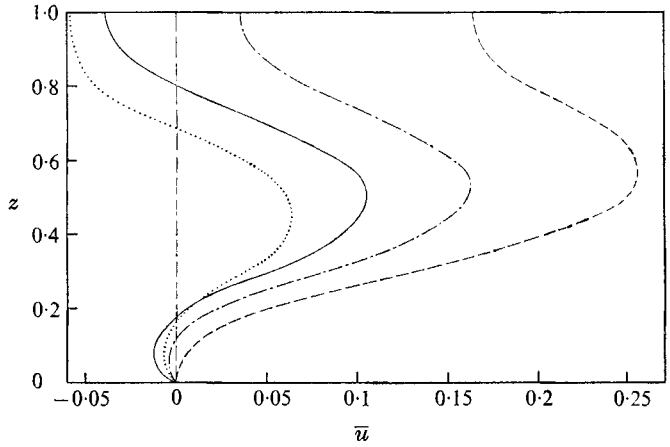

FIGURE 4. Time development of mean velocity for the free–rigid case $F = 100$, $S = 10$, $P = 0{\cdot}1$. Ratio of the actual time to the time taken to reach the steady state ($t \cong 12$): ....., $\frac{1}{12}$; ——, $\frac{1}{6}$; —·—, $\frac{1}{3}$; – – –, 1·0.

One property that all the profiles have in common is that there is no steady-state mean shear at a rigid surface (by definition of course there is none at a free surface). This is not true, however, during the transient flow period, during which the fluid is acquiring a net momentum. Figure 4 shows an example of the time development of the mean velocity profile during the transient period, the example being the free–rigid case with $F = 100$ and $P = 0{\cdot}1$. Note that the mean flow, and in particular the mean shear, is negative adjacent to the lower boundary before the steady state is reached. If the fluid is to acquire a net positive momentum through viscous interaction with a rigid surface, the rigid surface must exert a net positive force on the fluid. If the rigid surface corresponds to the lower boundary, this is accomplished by having a negative shear there, as can be easily seen from (3.4). By noting that $\psi(1) = -\tilde{u}$ and $\bar{\Omega} = d\bar{u}/dz$, we get in the rigid–rigid case, using the symmetry mentioned before,

$$\frac{\partial \tilde{u}}{\partial t} = \frac{-2}{S}\frac{d\bar{u}}{dz}\bigg|_{z=0}.$$

In the free–rigid case $\Omega(1) = 0$, hence

$$\frac{\partial \tilde{u}}{\partial t} = -\frac{1}{S}\frac{d\bar{u}}{dz}\bigg|_{z=0}.$$

Thus, if $\partial\tilde{u}/\partial t$ is positive, i.e. if the time rate of change of the net momentum in the fluid is positive, then $d\bar{u}/dz$ at $z = 0$ must be negative.

From figure 4 it is seen that early in the transient period the mean velocity is negative in the upper portions of fluid as well as near the rigid boundary. In the initial stages of flow development, near the top of the fluid thermal tilting of the convection cells produces negative Reynolds stresses, and hence a negative $\bar{u}$. As positive momentum diffuses up from the lower boundary, $\bar{u}$ near the top gradually becomes positive, reaching its steady-state value on a time scale close to the viscous diffusion time of the fluid layer. The symmetric cases reach steady

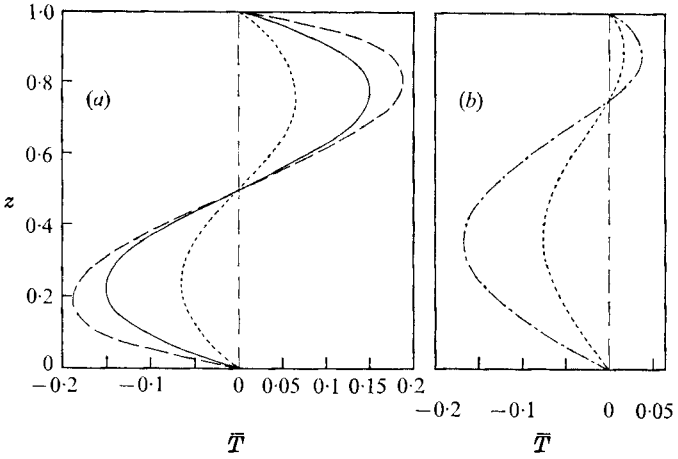

FIGURE 5. Steady-state mean temperature profiles at $F = 100$. (*a*) — — — —, free–free, $P = 1{\cdot}0$; ————, rigid–rigid, $P = 1{\cdot}0$; - - - - - -, rigid–rigid, $P = 0{\cdot}1$. (*b*) — — —, free–rigid, $P = 0{\cdot}3$; - - - - - -, free–rigid, $P = 0{\cdot}1$.

state considerably faster, because by symmetry the momentum has to diffuse only to the channel centre.

In the steady state, the dimensionless form of (2.7) can be integrated once to give

$$\frac{1}{SP}\frac{d\bar{T}}{dz} = \overline{wT} + c, \tag{5.1}$$

$$c = -\int_0^1 \overline{wT}\,dz. \tag{5.2}$$

Thus the mean temperature gradient at the boundaries is directly proportional to the net amount of work done by the buoyancy force per unit time.

Figure 5 shows mean temperature profiles for the same cases as in figure 3. Over most of the fluid layer there is a stabilizing mean temperature gradient, the exceptional regions being adjacent to the boundaries. The maximum absolute value of $\bar{T}$ does not always increase as the quantity SP increases, but does so only when SP is 'small'. As SP becomes large, thermal boundary layers begin to form. The fluctuating temperature is then damped in the interior of the fluid, and from (5.1) the mean temperature gradient, and hence mean temperature, is small in the interior, $\bar{T}$ being identically zero at the boundaries.

6. Steady-state streamlines and temperature fields

In this section we show steady-state streamline patterns and temperature fields in the fixed reference frame of the horizontal boundaries. The flow patterns and isotherms are displayed at the instant when the phase of the thermal wave is zero at $x = 0$. The temporal behaviour in the fixed frame is a convection of the whole pattern to the left with unit velocity, i.e. $\psi = \psi(x+t, z)$. The small number beside each streamline in figures 6–8 is the value of ψ along the streamline, and the arrows indicate the fluid velocity direction. The bottom surface corresponds

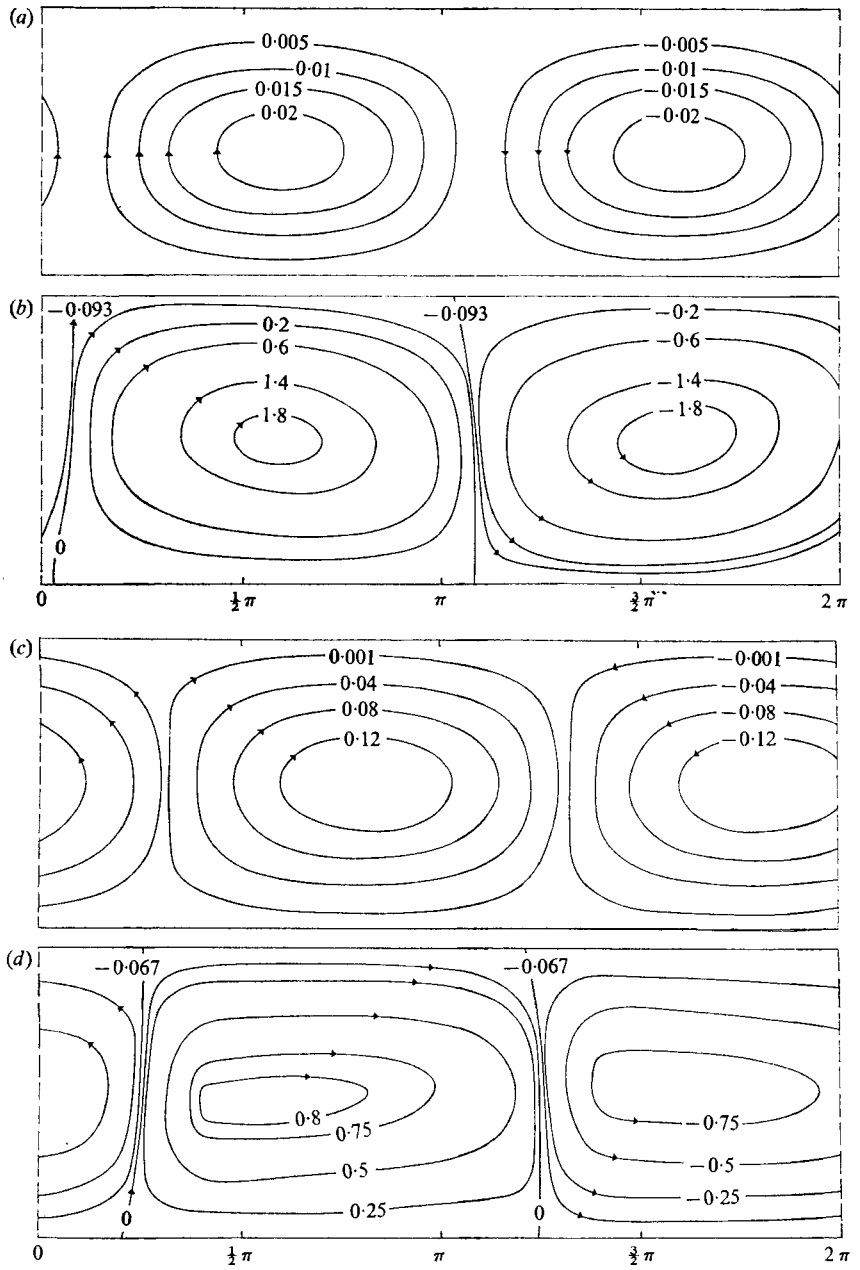

FIGURE 6. Steady-state streamlines as function of F for rigid–rigid boundary conditions. (*a*) $F = 1{\cdot}0$, $P = 0{\cdot}1$. (*b*) $F = 100$, $P = 0{\cdot}1$. (*c*) $F = 1{\cdot}0$, $P = 1{\cdot}0$. (*d*) $F = 100$, $P = 1{\cdot}0$.

to $\psi = 0$, while the upper surface has a constant value consistent with the vertically averaged mean flow. Because the aspect ratio β is 10^{-2} it was necessary to distort the geometry when displaying the flow patterns. The reader should keep this in mind when comparing vertical and horizontal length scales over which variations in the flow pattern occur. The same comments apply to the temperature fields displayed later in this section.

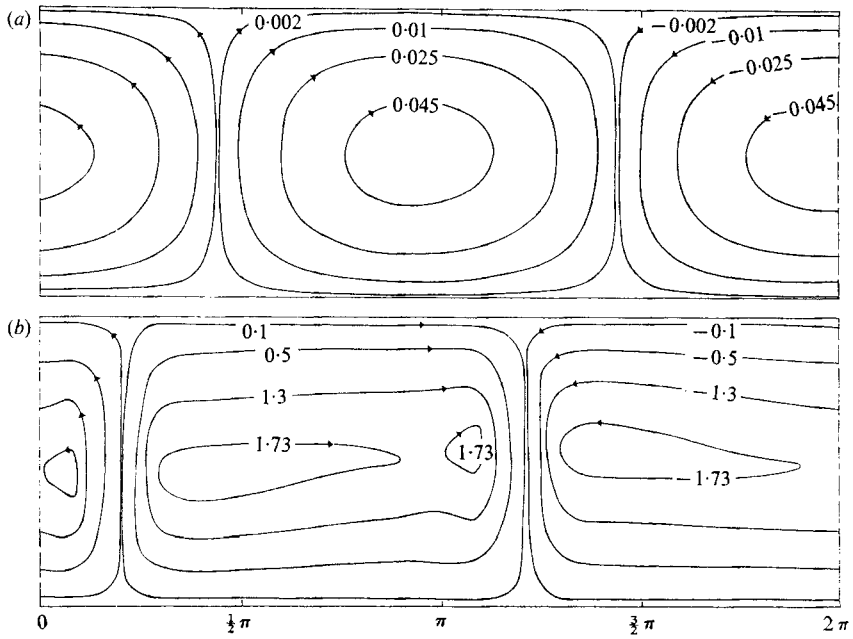

FIGURE 7. Steady-state streamlines as function of F for free–free boundary conditions with $P = 1{\cdot}0$. (*a*) $F = 1{\cdot}0$. (*b*) $F = 100$.

Whenever there is a net momentum within the fluid layer, so that the top surface does not correspond to $\psi = 0$, open streamlines exist. (Only closed streamlines are shown in certain instances where the mean velocity is quite small.) The dividing streamlines which separate the closed streamlines from the open ones are $\psi = 0$ and $\psi = \psi(1)$. These two streamlines define a 'channel', shown in most of the streamline figures, through which the entire net horizontal mass transport of the fluid occurs, i.e. if one integrates the horizontal velocity over a vertical cross-section of the fluid layer from $z = 0$ to 1, the net horizontal mass transport (or net momentum) is the same as if one had just integrated across the 'channel' defined by the dividing streamlines $\psi = 0$ and $\psi = \psi(1)$. It should be noted this latter region does not always consist of the same fluid particles, since ψ is time dependent.

6.1. *Nonlinear distortion of convection cells*

Figures 6 (*a*) and (*b*) compare the streamline patterns at $F = 1{\cdot}0$ and $F = 100$ for rigid–rigid boundary conditions at $P = 0{\cdot}1$. Figures 6 (*c*) and (*d*) present a similar comparison for the case $P = 1{\cdot}0$. The amplitudes of the velocity components, fluctuating and mean, are discussed later (see figures 14 and 15, which give plots of peak amplitude of the horizontal velocity fluctuation and magnitude of the mean flow as functions of F). It can be seen from figures 6 (*a*) and (*c*) that the streamline patterns for $P = 0{\cdot}1$ and $1{\cdot}0$ appear similar when $F = 1{\cdot}0$, although there is a larger phase lag of the flow pattern when $P = 1{\cdot}0$. However, at $F = 100$ the streamlines for each Prandtl number do become significantly different in appearance. The $P = 0{\cdot}1$ convection cells (figure 6 (*b*)) are inclined towards the

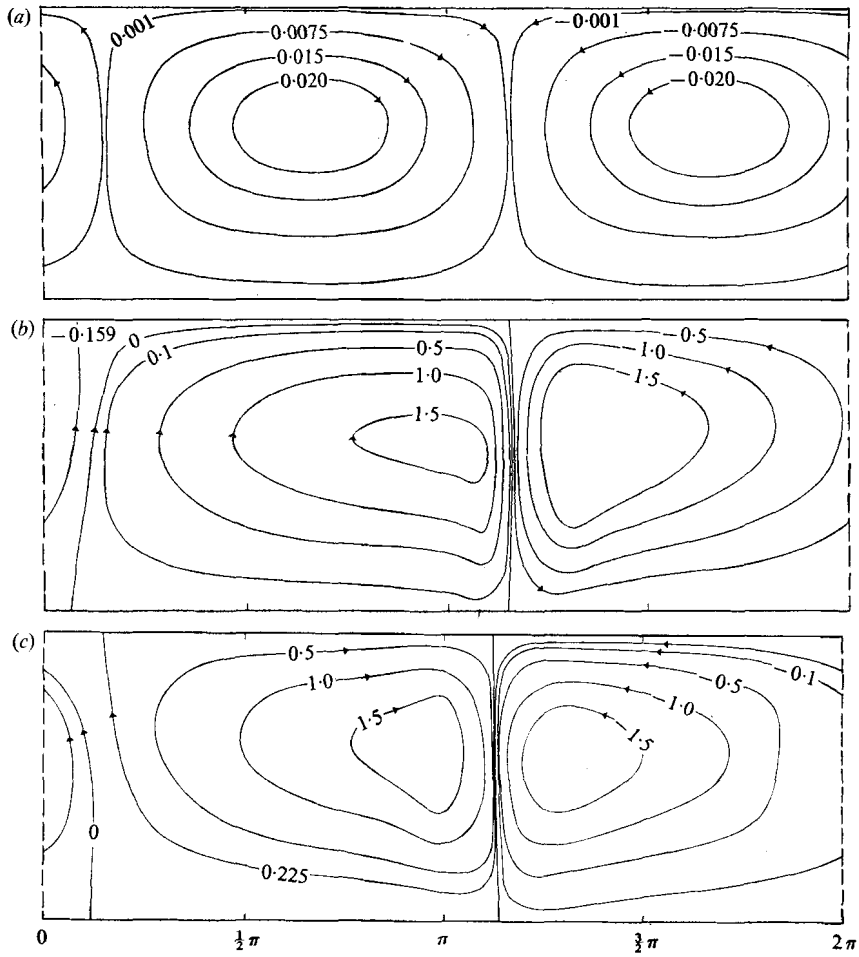

FIGURE 8. Steady-state streamlines as function of F for free–rigid boundary conditions. (*a*) $F = 1{\cdot}0$, $P = 0{\cdot}1$ (for $P = 0{\cdot}3$ streamlines are very similar). (*b*) $F = 100$, $P = 0{\cdot}1$. (*c*) $F = 100$, $P = 0{\cdot}3$.

descending region and this trend becomes more pronounced as F is increased beyond 100; when $P = 1{\cdot}0$ (figure 6 (*d*)) there is a small inclination away from the descending region. The phase lag for either value of P does not seem to be a very sensitive function of F.

The effect of F on the streamline pattern at constant S and P for free–free boundary conditions is shown in figure 7. The inclination of the convection cells at $F = 100$ is small, but in the same sense as that of the corresponding rigid–rigid case. There is a larger phase lag of the flow when F is moderately large than there is for rigid–rigid boundary conditions, but as F increases to about 100 the phase lag is approximately the same as for the corresponding cases.

Perhaps the most interesting of the three sets of flow patterns are the free–rigid streamlines as a function of F shown in figure 8 for $P = 0{\cdot}1$ and $0{\cdot}3$. These streamline contours change quite noticeably as the flow becomes nonlinear. At $F = 1{\cdot}0$ the flow pattern appears similar to those of the other sets of boundary

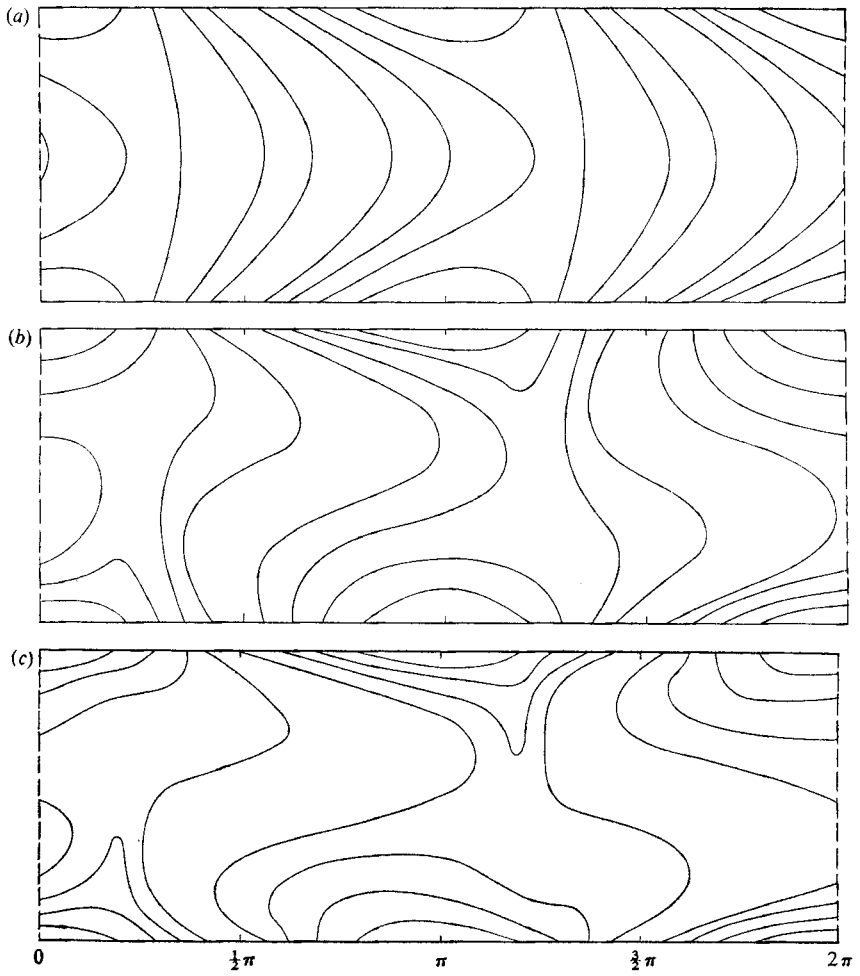

FIGURE 9. Steady-state isotherms as function of F with $P = 1{\cdot}0$. (*a*) Rigid–rigid, $F = 1{\cdot}0$. Because at $F = 1{\cdot}0$ the solution is essentially linear, free–free isotherms are the same. (*b*) Rigid–rigid, $F = 100$. (*c*) Free–free, $F = 100$.

conditions although because of the free–rigid boundary conditions there is a noticeable concentration of the streamlines near the top of the fluid layer. At $F = 100$ nonlinear interactions have caused the streamlines to be even more compressed near the top of the layer; the descending region has become quite narrow, while the upwelling region is spread broadly over the remainder of the interval between $x = 0$ and 2π. Such behaviour is consistent with results of Goody & Robinson (1966) and de Rivas (1971). The narrow descending region and broad upwelling region are the result of heating only at the top, while the concentration of the streamlines at the top is due to the free surface. The phase lag of the flow is not sensitive to increases in F.

There has been some discussion in the literature about how the finite rate of momentum and thermal diffusion acts to produce a tilt in the convection cells when the thermal wave is moving (see, for example, Schubert *et al.* 1970; Hinch &

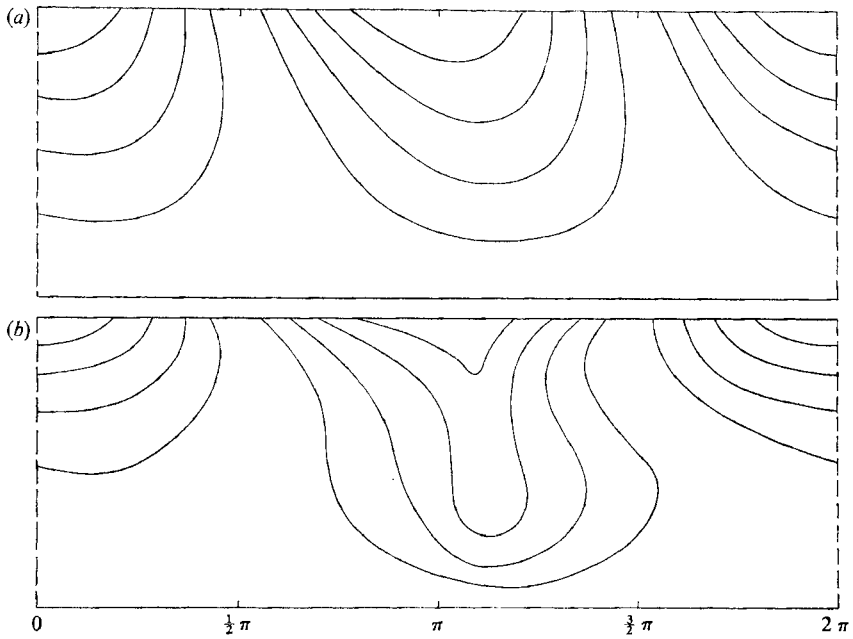

FIGURE 10. Steady-state isotherms as function of F for free–rigid boundary conditions with $P = 0{\cdot}3$. (*a*) $F = 1{\cdot}0$. (*b*) $F = 100$.

Schubert 1971). Such discussions have been for linear cases, or situations where the mean flow was much greater than the velocity fluctuations. This characteristic tilt in the convection cells caused by diffusion produces a correlation between the horizontal and vertical velocity components, i.e. a Reynolds stress. On the average, horizontal momentum is vertically advected in a direction which depends on the sense of the tilt of the cell, the sign of the mean shear being determined by (2.6). (When $F = 1{\cdot}0$ the cells appear to have no tilt at all, because the mean flow is quite small.)

This simple picture of the convection cells is no longer valid when the velocity fluctuations are larger than the thermal wave phase speed and the mean flow. In the interior of the fluid the fluctuating part of the nonlinear interactions is the dominant mechanism shaping the convection cells, and, as can be seen from the nonlinear streamline patterns just presented, the orientation of the streamlines is not always that expected on the basis of the diffusive mechanism discussed above. Nevertheless, when an average over a wavelength is taken, there is a net transport of horizontal momentum in the direction of the mean shear, consistent with (2.6). Thus the existence or non-existence of a significant mean flow cannot always be determined simply by observing the shape or orientation of the convection cells. This last comment does not apply to the dividing streamlines, from which both the existence and direction of a mean flow can be deduced.

Isotherms from representative examples for each set of boundary conditions are shown in figures 9 and 10. The contours are spaced at intervals of 0·2 (the contour corresponding to $T = 0$ is not shown) with a range from $-0{\cdot}8$ to 0·8. In the case $F = 1$ (figures 9(*a*) and 10(*a*)) the isotherms exhibit a characteristic

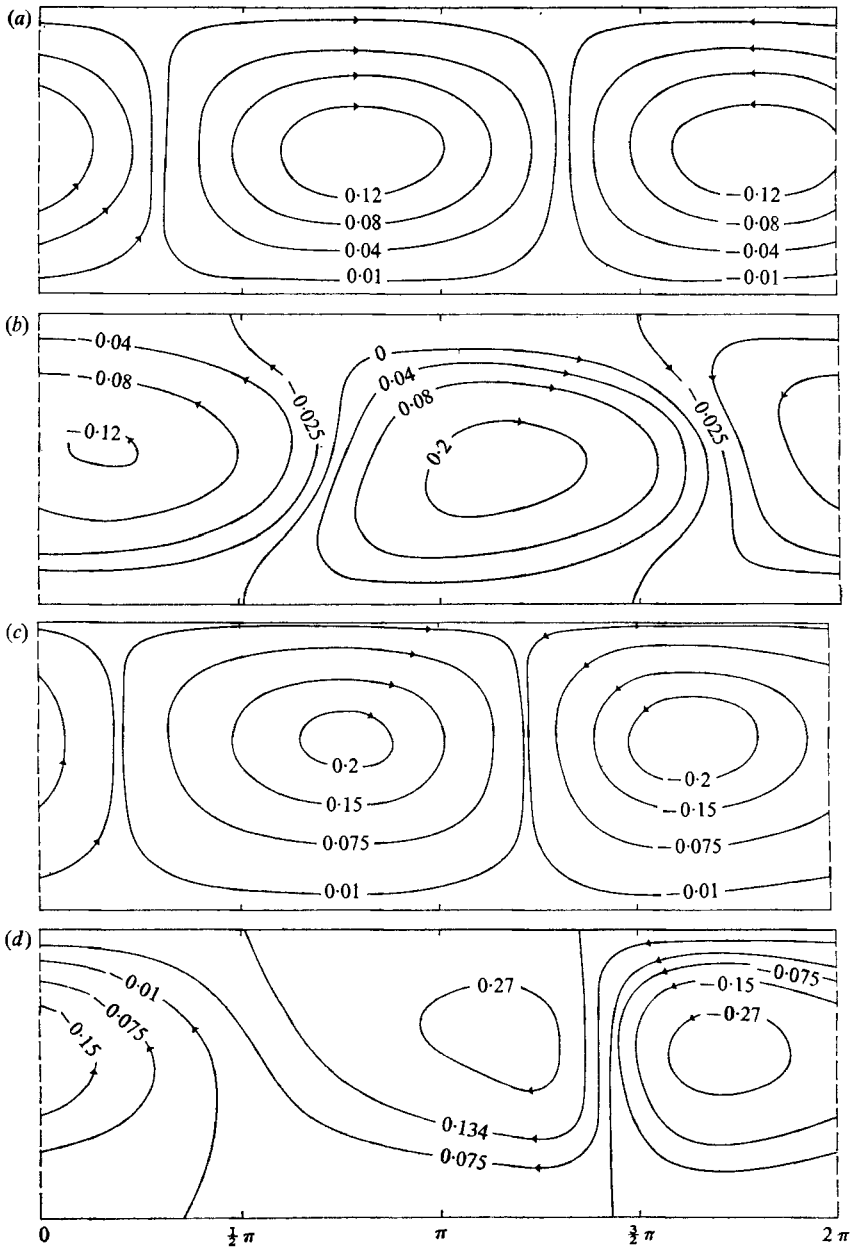

FIGURE 11. Comparison of streamline patterns at $S = 10$ and $S = 50$ with $F = 10$. (*a*) Rigid–rigid, $S = 10$, $P = 1{\cdot}0$. (*b*) Rigid–rigid, $S = 50$, $P = 1{\cdot}0$. (*c*) Free–rigid, $S = 10$, $P = 0{\cdot}3$. (*d*) Free–rigid, $S = 50$, $P = 0{\cdot}3$.

tilt, which is due to the thermal wave motion, i.e. there is a phase lag in temperature in the interior of the fluid because of the finite thermal diffusion time from the boundaries to any interior point. At $F = 100$ (figures 9(*b*), 9(*c*) and 10(*b*)), the velocity fluctuations have become large enough noticeably to affect the isotherms and, as expected, if one refers to the appropriate flow pattern the distortion in the

isotherms is seen to correlate with the sense of the fluid velocity. For example, the narrowing of the downwelling regions in both the free–rigid case (figure 10(*b*)) and the free–free case (figure 9(*c*)) is indicated by pinching of the isotherms in these regions. Similarly the narrowness of the upwelling regions in the free–free case (figure 9(*c*)) is apparent.

We conclude this subsection with a brief mention of the effect of the parameter S on the flow field. Figure 11(*a*) shows the rigid–rigid case with $F = 10$, $S = 10$ and $P = 1{\cdot}0$. This is to be compared with figure 11(*b*), which is for the same conditions but with $S = 50$. Figure 11(*c*) is the free–rigid case with $F = 10$, $S = 10$ and $P = 0{\cdot}3$, and should be compared with figure 11(*d*), which again is the same case except that $S = 50$. The reason for not showing the $S = 50$ cases at $F = 100$ is because the $F = 100$ cases did not reach the steady state. Such non-steady situations will be discussed in § 8. It is clear from figure 11 that the phase lag of the flow pattern increases significantly as S increases from 10 to 50. At smaller values of the Prandtl number, however, the increase in the phase lag is less. Also apparent from figure 11 is the presence of shear layers at $S = 50$. For smaller values of S ($S = 10$ say) such shear layers are found only at higher values of F.

6.2. *Comparison of stationary and moving thermal sources*

Figure 12 shows nonlinear streamlines for each of the three sets of boundary conditions when the thermal wave is stationary and there is no mean flow. (In these cases the equations were non-dimensionalized in exactly the same way as when the thermal wave was moving, e.g. velocities were non-dimensionalized with u_0, etc. Such a non-dimensionalization is convenient for comparison purposes.) It is important to note that in each of these examples the applied thermal wave is symmetric about some phase of the wave, for example, $x = 0$, 2π, etc. During the course of this investigation it has become apparent that there exist other quite general situations where stationary periodic thermal sources do in fact create mean flows. (Such possibilities were suggested to us by F. H. Busse and J. Whitehead.) We shall discuss these situations later in this section, but suffice it to point out here that in such cases the thermal source does not have any phase about which there is symmetry.

Two significant differences should be noted between the stationary streamline patterns in figure 12 and the patterns when the thermal wave is moving. When $\overline{u} \equiv 0$, all the streamlines are closed and are mirror images of each other about $x = \pi$. When the thermal wave is moving and $\overline{u} \not\equiv 0$, a phase lag exists between the flow pattern and the thermal wave, the amount varying with boundary conditions and parameter values. Further, all the streamlines are not closed, as was discussed at the beginning of this section.

Apart from these general differences between the situations where $\overline{u}$ is or is not identically zero, there exist some interesting individual contrasts. For example, when $F = 100$ and $P = 1{\cdot}0$ (figure 12(*b*)) the streamlines when $\overline{u} \equiv 0$ have relatively thin descending and ascending regions, and small eddies have developed in the interior of the convection cell (only the eddy in the centre of the cell is shown). The presence of these small eddies has been confirmed by refining the grids. Similar interior eddies have been observed in natural convection flows in

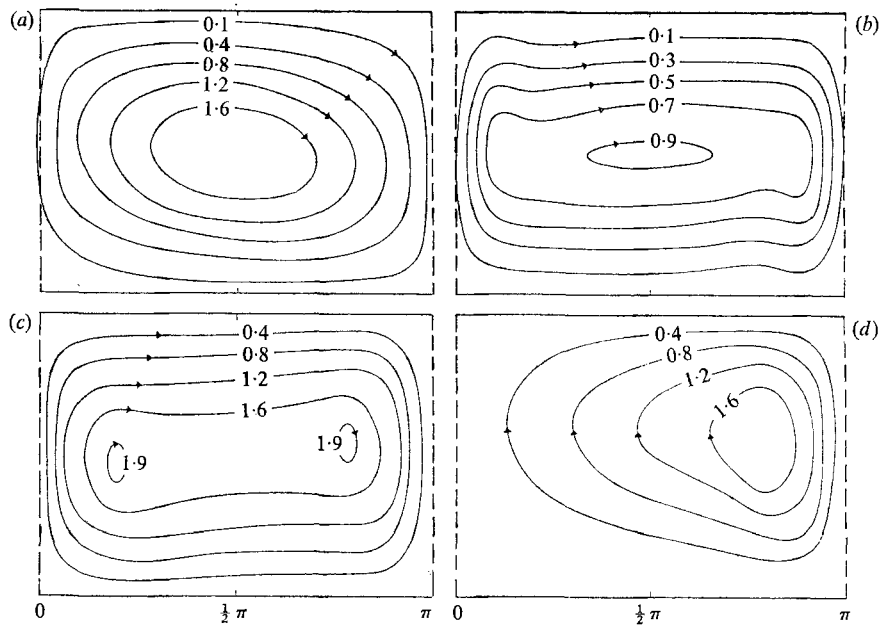

FIGURE 12. Steady-state streamlines when thermal wave is stationary for $F = 100$. Only one-half of the pattern is shown in each case because of mirror symmetry about $x = \pi$. $F = 100$. (*a*) Rigid–rigid, $P = 0{\cdot}1$. (*b*) Rigid–rigid, $P = 1{\cdot}0$. (*c*) Free–free, $P = 1{\cdot}0$. (*d*) Free–rigid, $P = 0{\cdot}3$.

enclosures by de Vahl Davis (1968). The corresponding situation when $\overline{u} \not\equiv 0$ (figure 6(*d*)) has fairly broad upwelling and downwelling regions and no small eddies, but it should be noticed that the right convection cell has a much narrower descending region than does the left cell. Similarly, the ascending portion of the left cell is much narrower than that of the right cell. It can be seen from figures 12(*a*) and 6(*b*) that when $P = 0{\cdot}1$ there is little difference in appearance between the zero and non-zero $\overline{u}$ streamlines at the same values of F and S (apart from the general differences discussed above).

Because there is no net momentum within the fluid layer for free–free boundary conditions, and $\overline{u}$ is smaller in magnitude than the fluctuations, all the streamlines are closed even when the thermal wave is moving. The flow pattern when $\overline{u} \equiv 0$ is shown in figure 12(*c*); and as in the rigid–rigid $\overline{u} \equiv 0$ case the descending and ascending regions are rather narrow, small eddies having formed in the interior of the convection cell. Unlike the rigid–rigid case, however, the $\overline{u} \not\equiv 0$ streamlines at $F = 100$ (figure 7(*b*)) exhibit the same thinness in the up- and downwelling regions as do the streamlines for $\overline{u} \equiv 0$.

Figure 12(*d*) shows the streamline pattern for free–rigid boundary conditions at $F = 100$ and $P = 0{\cdot}3$ when $\overline{u} \equiv 0$, and can be compared with figure 8(*c*), which is the same case when $\overline{u} \not\equiv 0$.

In the nonlinear free–rigid flow patterns there is a noticeable asymmetry about the descending region when the thermal source is moving, especially when $P = 0{\cdot}1$ at $F = 100$, figure 8(*b*). This asymmetry is a purely nonlinear effect,

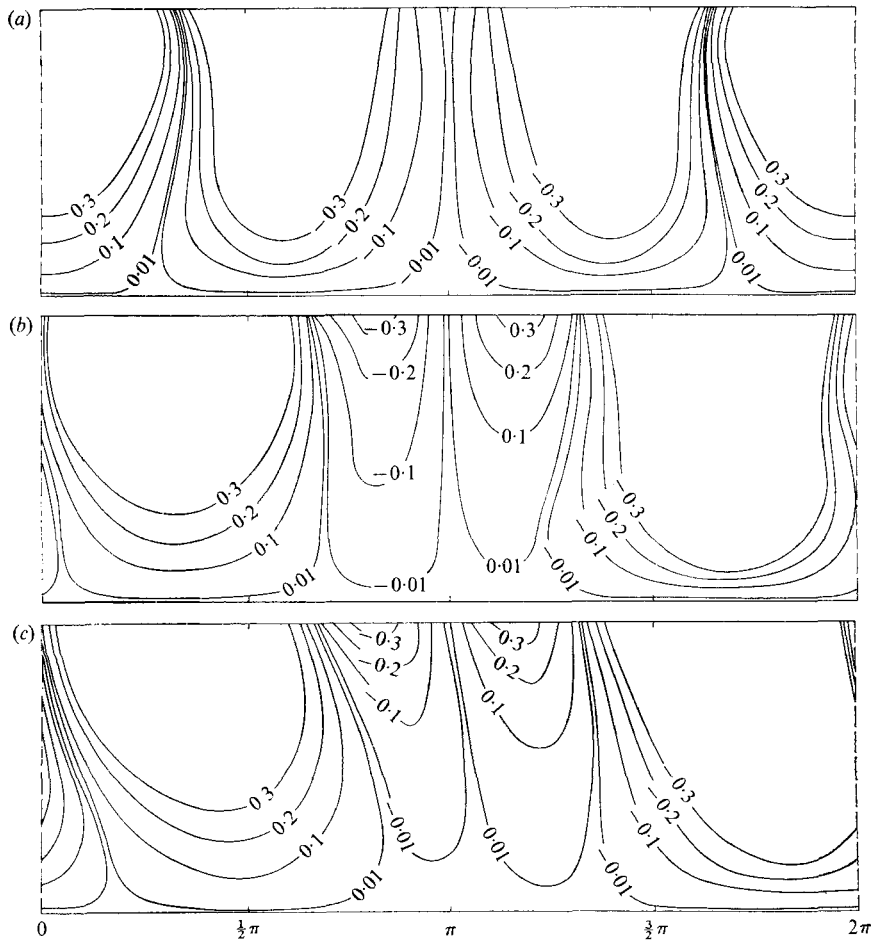

FIGURE 13. Comparison of isotherms between stationary symmetric and asymmetric thermal sources and between stationary and moving asymmetric thermal sources. Free–rigid case, $F = 10$, $P = 0{\cdot}3$, $Re = u_0 d/\nu = 1000$. (*a*) $T = \cos x + \cos 2x$ at $z = 1$. (*b*) $T = \sin x + \sin 2x$ at $z = 1$. (*c*) $T = \sin(x+t) + \sin 2(x+t)$ at $z = 1$.

since at $F = 1{\cdot}0$ (figure 8(*a*)) the two convection cells on either side of the downwelling region do not exhibit such a pronounced asymmetry. At $F = 100$, $\bar{u}(1)$ is positive at $P = 0{\cdot}1$ but negative at $P = 0{\cdot}3$. In figures 8(*b*) and (*c*) it can be seen that the 'channel' consisting of the open streamlines is consistent with the sense of the mean flow.

We briefly mentioned above that certain stationary thermal sources could generate mean velocities. To understand how this occurs, recall that a tilt in the isotherms tends to tilt the convection cells, thereby creating a Reynolds stress. As long as the isotherms are tilted, by whatever mechanism, a non-zero Reynolds stress can be expected. If a periodic stationary thermal forcing which is not symmetric about any phase is applied, the isotherms are tilted and a mean flow is generated.

For example, we have considered the following two stationary cases for free–rigid boundary conditions:

$$\text{(i)}\quad T = \begin{cases} \cos x + \cos 2x & \text{at} \quad z = 1, \\ 0 & \text{at} \quad z = 0; \end{cases}$$

$$\text{(ii)}\quad T = \begin{cases} \sin x + \sin 2x & \text{at} \quad z = 1, \\ 0 & \text{at} \quad z = 0. \end{cases}$$

In the first case, as in the stationary cases discussed above, no mean flow is produced. The reason is that there is symmetry about $x = 0$, π, 2π, etc. Thus the effect of any tilting or skewing of the isotherms on one side of $x = \pi$, say, is completely cancelled by the opposite tilting or skewing of the isotherms on the other side of $x = \pi$. This is illustrated for the first case in figure 13 (*a*). However, in the second case there is no symmetry about any phase, and there is a net effect produced by any tilt or skewness of the isotherms (shown in figure 13 (*b*)). From figure 13 (*b*) one would expect a mean velocity to be generated in the positive x direction, and such is in fact the case. The phase difference between the horizontal and vertical fluctuating velocities necessary to produce a Reynolds stress arises principally from the nonlinear convective terms of the vorticity equation. This is in contrast to the situation where the thermal source is moving, and thermal and momentum diffusion play important roles in creating the required phase difference. This point is illustrated in figure 13 (*c*), which shows the effect of moving the applied thermal wave in the case of the second of the above sets of boundary conditions, i.e. $T = \sin(x+t) + \sin 2(x+t)$ at $z = 1$. In this instance thermal diffusion has tilted the isotherms to the left, and a negative mean velocity is generated. Note that the tilt of the isotherms in figure 13 (*c*) is much more apparent than in figure 13 (*b*), indicating that diffusive effects clearly dominate when the source is moving, at least at the value $F = 10$ for which the examples in figure 13 were computed. The magnitude of the mean velocity is a few per cent of the phase speed of the thermal wave when the source is moving and is of the same order of magnitude when the source is stationary.

7. Parameter dependence of velocity components

Figures 14 and 15 show plots of mean ($\bar{u}, \tilde{u}$) and fluctuating velocity (u') as a function of F for various values of P. A very interesting aspect of these figures is that in practically all cases the linear expressions for the mean flow and maximum absolute value of the horizontal fluctuating velocity have a larger region of validity than one would anticipate. Linear theory is strictly justifiable only when the fluctuating components of the velocity, and hence the mean flow, are considerably smaller than the phase speed of the thermal wave. In the examples, however, when $F = 10$ the horizontal fluctuation reaches magnitudes of the order of the wave speed, but evidently the fluctuating parts of the nonlinear interactions do not yet significantly affect the average properties of the flow. Most of the examples do, however, deviate significantly from an F^2 proportionality before $\bar{u}$ reaches unity, the exception being the free–rigid case where

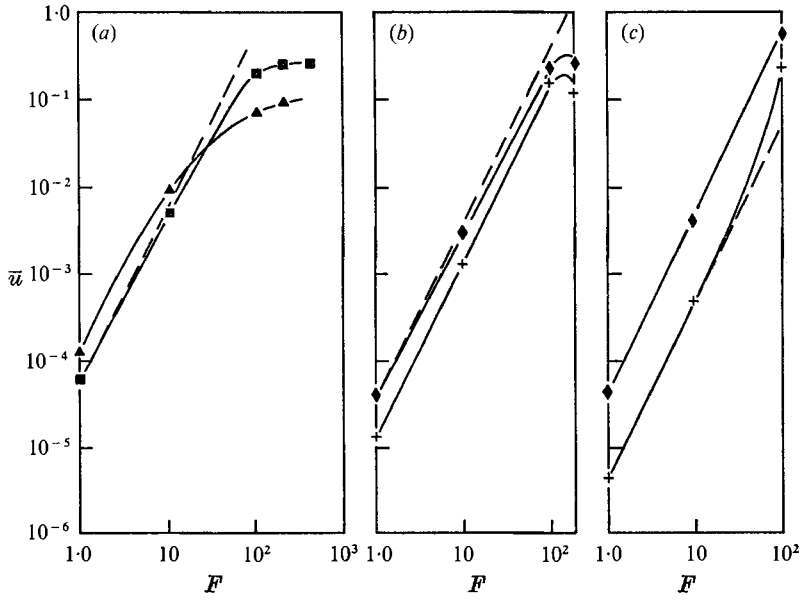

FIGURE 14. Mean velocity as function of F. – – –, F^2 dependence. (*a*) Mean velocity at channel centre: ■, rigid–rigid, $P = 0{\cdot}1$; ▲, free–free, $P = 1{\cdot}0$. (*b*) Free–rigid, $P = 0{\cdot}1$: ◆, $\bar{u}_{\max}$; +, $\tilde{u}$. (*c*) Free–rigid, $P = 0{\cdot}3$: ◆, $|\bar{u}_{\max}|$; +, $|\tilde{u}|$.

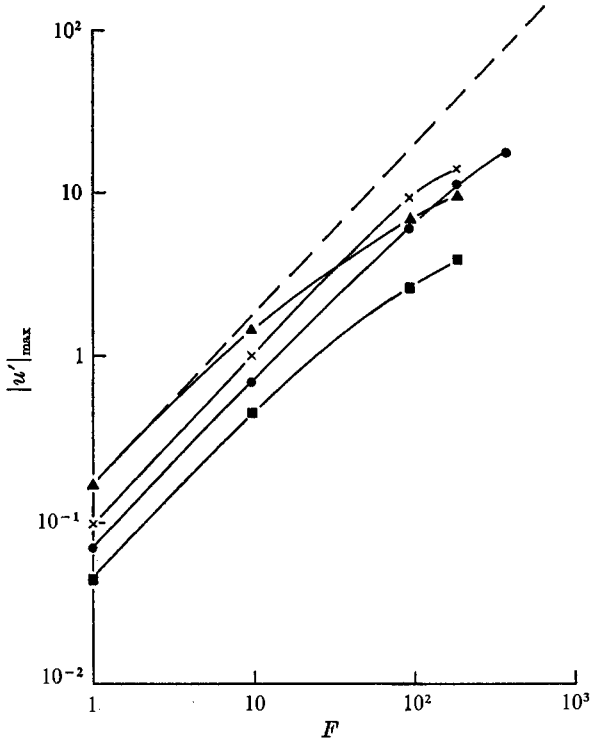

FIGURE 15. Maximum amplitude of horizontal velocity fluctuation as function of F. – – –, F dependence. ×, free–rigid, $P = 0{\cdot}1$ ($P = 0{\cdot}3$ essentially the same); ▲, free–free, $P = 1{\cdot}0$; ●, rigid–rigid, $P = 0{\cdot}1$; ■, rigid–rigid, $P = 1{\cdot}0$.

$P = 0{\cdot}3$. (Calculations at $P = 0{\cdot}3$ with $S = 20$ or 50 did not reach the steady state at $F = 100$.)

In the free–free example the departure of $\bar{u}$ from the F^2 law is fairly smooth, but in the rigid–rigid case there appears to be a rather abrupt transition at $F \sim 100$. The relatively rapid deviation of $\tilde{u}$ from the F^2 proportionality above $F = 100$ when $P = 0{\cdot}1$ in the free–rigid case is a consequence of nonlinear effects on the value of the critical Prandtl number (see below). Although $|\bar{u}_{\max}|$ obeys the F^2 dependence up to $F = 100$ when $P = 0{\cdot}3$ (at $F = 200$ the steady state was not reached), the vertically averaged mean flow $|\tilde{u}|$ increases in magnitude faster than F^2 for $F \gtrsim 100$. Even though $\tilde{u}$ is negative when $P = 0{\cdot}3$, at values of $F \sim 10$ a substantial part of the mean flow profile is positive. As F increases, less and less of the profile is positive, and hence the magnitude of $\tilde{u}$ increases faster than F^2 in this region.

In all the numerical cases the maximum amplitude of the horizontal velocity fluctuation was significantly greater than the mean flow magnitude. If the fluctuating nonlinear terms in (2.13) are balanced against the buoyancy term when F is large, one expects the velocity fluctuation in the interior of the fluid to be roughly proportional to $F^{\frac{1}{2}}$ (assuming there are no thin fast regions), which in fact is fairly close to the numerical results when $F \lesssim 100$. At most, the mean flow might be proportional to F, but as F, and subsequently the velocity fluctuations, become large, nonlinear boundary or shear layers form whose thickness and internal behaviour depend on F. Since the mean flow depends on the phase difference between the horizontal and vertical velocity fluctuations as well as their magnitudes, the mean flow is likely to be proportional to some power of F less than unity. For example, on the basis of crude scaling arguments for boundary-layer thickness (Hinch 1971) etc., for rigid–rigid boundary conditions $\bar{u}$ is estimated to be proportional to approximately $F^{\frac{2}{5}}$ when F is large.

For the parameter values considered the mean flow is only slightly dependent on Prandtl number in the rigid–rigid and free–free cases. On the other hand the peak magnitudes of the velocity fluctuations when $P = 0{\cdot}1$ are about 1·5 times the values when $P = 1{\cdot}0$. The reason why the mean flow is not considerably larger when $P = 0{\cdot}1$ than when $P = 1{\cdot}0$ lies in the fact that the thermal phase lag, which depends on SP, is much less for $P = 0{\cdot}1$. The smaller thermal phase lag tends to cause a smaller Reynolds stress because the isotherms are not tilted as much and this effect evidently compensates for the larger magnitudes of the velocity fluctuations when $P = 0{\cdot}1$.

As was discussed before, depending on the value of S, the vertically averaged mean flow in the free–rigid case can change sign between $P = 0{\cdot}1$ and $P = 0{\cdot}3$. In the linear case the critical value of P is independent of F, independent of S when S is small, and proportional to $S^{-\frac{3}{2}}$ when S is large. As F increases and nonlinear effects become important the critical value of P becomes a function of F as well as of S. For example, at $S = 20$, $P = 0{\cdot}1$ with $F \lesssim 10$, $\tilde{u}$ is still positive but when $F \sim 100$, $\tilde{u}$ is negative. When $S = 10$, $\tilde{u}$ is still positive at $F = 200$, indicating that the larger the value of S, the smaller F has to be to cause a reversal in the net momentum within the fluid.

The S dependence of $\bar{u}$ for the parameter values considered in this paper ranged

between approximately S and S^2, depending on the particular case. At the higher values of S, i.e. $S \sim 50$, the steady state was not usually achieved when $F \sim 100$. The reasons for this will be discussed in the next section. The velocity fluctuations are rather insensitive to S, increasing by only about 20–30 % at a given F as S is increased from 10 to 50.

8. Non-steady cases

A survey of those cases which did not reach the steady state reveals that each occurred in the upper part of the range of at least two of the parameters F, S or P. We have presented no results from these cases because it is probable that numerical truncation errors caused the oscillatory behaviour. Consider the temperature equation. Regardless of which finite-difference form of the horizontal advective term mentioned in the numerical description is used there is a term of $O(\Delta x)$ which represents a false diffusion of heat, i.e. the differential equation equivalent to the finite-difference equation contains a term $\kappa_N \partial^2 T/\partial x^2$, where κ_N is the dimensionless coefficient arising from the numerical scheme and is proportional to the horizontal velocity as well as Δx. (See also the discussion in § 3.) At a given F, the larger the quantity SP, the smaller Δx must be in order that the term $\kappa_N \partial^2 T/\partial x^2$ be small compared with $(1/SP)\nabla_\beta^2 T$. Similarly, at a given value of SP, as F increases, and consequently the horizontal velocity increases, Δx must decrease to maintain accuracy. In the vorticity equation a similar numerical diffusion term exists and must be small compared with the right-hand side of (2.13). In most cases this is accomplished with a less restrictive Δx than that needed to make the energy equation accurate. When the numerical diffusion term is not small enough in either equation, it can prevent the steady state from being achieved. The obvious remedy of course is to refine the horizontal grid, but to do so effectively for the oscillatory cases would have required more computer time than we were willing to expend.

One further point should be mentioned. The Reynolds number Re based on the phase speed of the thermal-wave and fluid-layer thickness is equal to S/β. When $S = 50$, $Re = 5000$, and it is possible that even if numerical errors were not important the flow would be turbulent at high values of F.

9. Effects of initial conditions

Thus far in the discussion we have considered only the examples which had quiescent initial conditions. Thompson (1970) investigated numerically a nonlinear instability mechanism which indicated that initial conditions could be important in determining the final steady-state mean velocity. Under very special circumstances, Busse (1970) has obtained two solutions to the full nonlinear equations, each solution being for exactly the same set of parameter values and boundary conditions. One of the solutions has an associated mean velocity, the other has none. Presumably the solution which a fluid chooses depends on the initial conditions.

In an attempt to ascertain how the steady-state flow field depends on the

initial fluid state, we imposed different initial mean velocity profiles as Thompson did. This was done for each set of boundary conditions at $F = 100$, $S = 10$ and the same values of P used previously. Some runs were made at $S = 100$ for free–free boundary conditions, but these runs were for relatively small values of F because of the effects discussed in the last section. The initial profiles had magnitudes comparable to, and in some cases significantly larger than, the amplitudes of the velocity fluctuations.

In all the examples for which the initial conditions were varied the flow eventually reached the same steady state as that obtained using quiescent initial conditions. It appears, therefore, that for the range of parameter values we have considered in this study the nonlinear instability suggested by Thompson does not occur, nor are initial conditions important in determining the steady-state flow field. It must be kept in mind, however, that we have treated only a limited number of initial states, and it is possible, although we do not believe it likely, that some other particular set of initial conditions could alter our conclusion.

10. Conclusions

The results we have obtained indicate that at small to medium values of S, i.e. $S \lesssim 50$, it appears unlikely that mean flows much larger than the phase speed of the thermal wave can be created, even at quite large values of the thermal forcing parameter F or small values of the Prandtl number P. [The only case which obeys the F^2 law up to $F = 100$ has $S = 10$ with $P = 0{\cdot}3$. At $F = 200$ the steady state was not reached, for reasons discussed above. It is likely, however, that once the entire mean velocity profile becomes negative (see discussion on the parameter dependence of the mean flow), the dependence on F should begin to decrease. This essentially occurs by the time $F = 100$.] Although we did not consider internal heating or an applied boundary heat flux it is unlikely that our conclusion would be altered in these situations. One effect we have not considered, and which might be important, is an applied static stratification. Kelly & Vreeman (1970) have shown for the linear regime that, when the frequency of the applied thermal wave is in resonance with the natural modes of oscillation of the fluid layer, Reynolds stresses produced by the internal waves can be the dominant mechanism creating the mean shear. We plan to investigate this phenomenon in the nonlinear regime in the near future. Thus, with the possible exception just mentioned, the only apparent situation in which it is possible to produce large mean flows is when the parameter S is large, perhaps with F simultaneously large.

The generation of mean velocities in a fluid in convective motion is in general associated with asymmetries of the thermal forcing (Busse 1970). The motion of a heat source introduces such an asymmetry, and because of the motion thermal and momentum diffusion play significant roles in creating the phase difference between the horizontal and vertical velocity fluctuations required to produce a Reynolds stress. If the thermal forcing is stationary but asymmetric, mean flows are generated, but in this situation the phase difference between the velocity components arises principally from the nonlinear advective terms.

Finally, the nonlinear streamline patterns indicate that the existence and direction of a significant mean velocity cannot necessarily be deduced from the shape or orientation of the convection cells.

We would like to thank F. H. Busse and J. A. Whitehead for many very enlightening and stimulating discussions. One of us (R. E. Y.) was supported during this work by NSF grant GA-19605.

REFERENCES

Busse, F. H. 1970 To be published.
Davey, A. 1967 *J. Fluid Mech.* **29**, 137.
De Rivas, E. 1971 Ph.D. thesis, M.I.T.
De Vahl Davis, G. 1968 *Int. J. Heat and Mass Transfer*, **11**, 1675.
Goody, R. M. & Robinson, A. 1966 *Astrophys. J.* **146**, 339.
Hinch, E. J. 1971 Smith and Rayleigh Prize Essay, University of Cambridge.
Hinch, E. J. & Schubert, G. 1971 *J. Fluid Mech.* **47**, 291.
Kelly, R. E. & Vreeman, J. D. 1970 *Z. angew. Math. Phys.* **21**, 1.
Malkus, W. V. R. 1970 *J. Atmos. Sci.* **27**, 529.
Schubert, G. 1969 *J. Atmos. Sci.* **26**, 767.
Schubert, G., Young, R. E. & Hinch, E. J. 1970 *J. Geophys. Res.* **76**, 2126.
Stern, M. E. 1959 *Tellus*, **11**, 175.
Thompson, R. 1970 *J. Atmos. Sci.* **27**, 1107.
Torrance, K. E. 1968 *J. Res. Nat. Bur. Stand. Math. Sci.* B **72**, 281.
Torrance, K. E. & Rockett, J. A. 1969 *J. Fluid Mech.* **36**, 33.
Whitehead, J. A. 1971 *Geophys. Fluid Dyn.* (in press).